JACS
JOURNAL OF THE AMERICAN CHEMICAL SOCIETY
Article
pubs.acs.org/JACS

Alkali Metal Control over N−N Cleavage in Iron Complexes

Katarzyna Grubel,[†] William W. Brennessel,[‡] Brandon Q. Mercado,[†] and Patrick L. Holland*[,†]

[†]Department of Chemistry, Yale University, New Haven, Connecticut 06511, United States
[‡]Department of Chemistry, University of Rochester, Rochester, New York 14627, United States

Supporting Information

ABSTRACT: Though N_2 cleavage on K-promoted Fe surfaces is important in the large-scale Haber−Bosch process, there is still ambiguity about the number of Fe atoms involved during the N−N cleaving step and the interactions responsible for the promoting ability of K. This work explores a molecular Fe system for N_2 reduction, particularly focusing on the differences in the results obtained using different alkali metals as reductants (Na, K, Rb, Cs). The products of these reactions feature new types of Fe−N_2 and Fe-nitride cores. Surprisingly, adding more equivalents of reductant to the system gives a product in which the N−N bond is not cleaved, indicating that the reducing power is not the most important factor that determines the extent of N_2 activation. On the other hand, the results suggest that the size of the alkali metal cation can control the number of Fe atoms that can approach N_2, which in turn controls the ability to achieve N_2 cleavage. The accumulated results indicate that cleaving the triple N−N bond to nitrides is facilitated by simultaneous approach of least three low-valent Fe atoms to a single molecule of N_2.

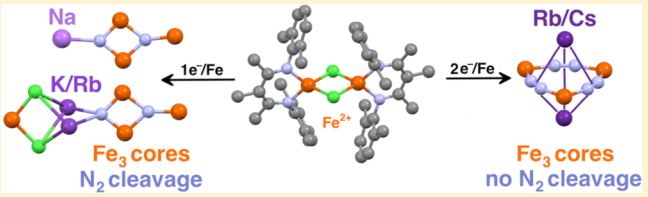

INTRODUCTION

The Haber−Bosch process, which supplies ammonia for fertilizers that support a significant fraction of the world's crops, is carried out predominantly on K-promoted Fe catalysts.[1,2] Under catalytic conditions, the surface iron atoms have an average oxidation state between 0 and +1.[3] The K additive is an "electronic promoter", and the positive charge is thought to draw electrons toward the surface, which weakens the binding of NH_3.[4] Most studies have used single-crystal iron faces because their surface structures are known.[3] The Fe(111) plane, which has the greatest atomic-scale roughness, is the most active for N_2 cleavage.[5] On this surface, N_2 cleavage (which is the rate-limiting step) takes place from an intermediate in which the bound N_2 has its N−N bond roughly parallel to the surface.[6] Calculations suggested a specific geometry for the transition state of N−N cleavage on Fe(111), in which N_2 is bound to several metal atoms.[7]

Biological nitrogen fixation also takes place at a site that has multiple iron atoms: the iron−molybdenum cofactor (FeMo-co) of nitrogenase.[8] Recent studies have established the structure and composition of the FeMoco.[9] Mutation of the nitrogenase enzyme has led to a series of variants, in which the relative activities of mutants suggest that N_2 and other substrates are reduced at a four-iron face of the FeMoco.[10] The importance of Fe sites in the FeMoco is supported by a recent crystal structure, which shows that CO inhibition involves binding of the CO molecule to two Fe atoms on the same face of the enzyme.[11] This implies that N_2 binding might also involve bridging sites, and heightens interest in understanding the fundamental behavior of multi-iron sites toward N_2.

Synthetic complexes offer a distinctive way of gaining insight into the steps involved in N−N bond cleavage, because it is possible to characterize their structures in detail and vary the Fe environment systematically. The trends and principles discovered during investigation of synthetic complexes lay the foundation for understanding the mechanism of N_2 cleavage on surfaces and in biological systems. In this Article, we address several important questions that relate particularly to the Fe surfaces that catalyze the Haber−Bosch process: (a) What is the smallest number of Fe atoms necessary to break the N−N bond into nitrides? (b) What oxidation level of Fe atoms is needed to bring about N−N bond scission? (c) Why is K the most effective alkali metal promoter?[12]

There have been numerous studies on iron-N_2 complexes.[13,14] However, there are only a few compounds with Fe atoms positioned close to each other that are able to address the above questions.[15] In previous work, we have shown that *binding* of N_2 can be assisted by K^+, both by electrostatic forces that improve backbonding into the π^* orbital of N_2, and by locking two Fe atoms in close proximity.[16,17] We have also reported the only Fe system that is capable of completely *cleaving* the N−N bond of N_2 to nitrides.[18,19] The product of this reaction (**1-K**, Scheme 1) contains four iron atoms and two K^+ ions coordinated to two nitrides. However, it is not yet clear whether K is unique in facilitating the N_2-cleaving reaction, and the nature of the cooperation between the transition metal and the alkali metal needs to be elucidated.

In this contribution, we address the above questions by varying the choice and amount of alkali metal in the N_2-

Received: July 22, 2014
Published: November 20, 2014

ACS Publications © 2014 American Chemical Society

dx.doi.org/10.1021/ja507442b | J. Am. Chem. Soc. 2014, 136, 16807−16816

Scheme 1. Binding and Reduction of N_2 in Multinuclear Iron Complexes[a]

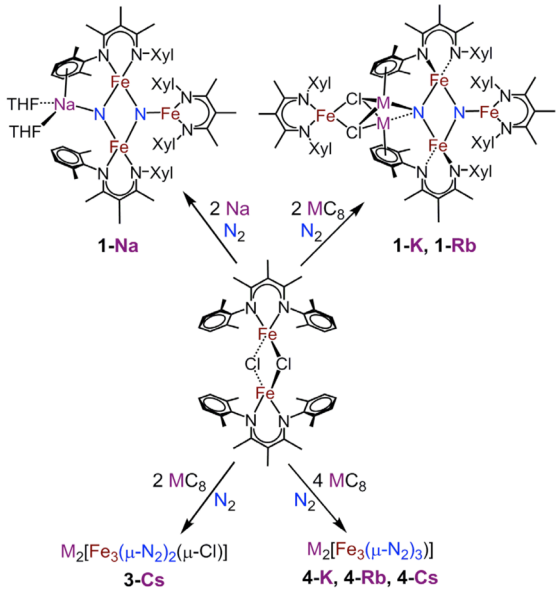

[a]The structures of compounds **3** and **4** are shown in Figures 4 and 5 below.

cleaving system. Interestingly, supplying the system with *more* electrons yields *less* N−N bond activation, and we offer an explanation for this counterintuitive trend. In addition, we describe a new type of triiron structure with three bridging N_2 units. Our results show the utility of alkali metals for influencing small-molecule reduction reactions, which complements a growing body of work in which alkali metal or Sc cations facilitate oxidation reactions.[20]

RESULTS

K and Rb Cleave N_2 to Give Fe_4−Nitride Complexes. Our survey of reductants has shown that the most effective reductants for diketiminate-iron(II) complexes are MC_8 (M = alkali metal), in which excess electrons lie on the graphite and the alkali metal cations are intercalated between the layers in a known stoichiometry.[21] In previously reported experiments, we treated a THF solution of $[LFe(\mu\text{-}Cl)]_2$ (L = 2,4-bis(2,6-dimethylphenylimino)-3-methylpent-3-yl) with 2 equiv of KC_8, which is the appropriate stoichiometry to reduce each iron(II) to the formally iron(I) oxidation level.[18] Under an N_2 atmosphere, the presumed transient iron(I) intermediates[22] perform the six-electron reduction of N_2 to two N^{3-}, which is balanced by the six-electron oxidation of four Fe^{1+} to 2 Fe^{2+} and 2 Fe^{3+} in the fully characterized product $[(LFe)_4Cl_2K_2N_2]$ (**1-K**, Scheme 1).

Since the oxidation product K^+ was a part of the final product structure, we anticipated that changing the reductant to RbC_8 might have an influence on the structure. Thus, in a new reaction we used Rb on graphite (RbC_8), which under analogous conditions gives **1-Rb** (Scheme 1). Specifically, a concentrated solution of the Fe^{2+} compound $[LFe(\mu\text{-}Cl)]_2$ was treated with 2 equiv of RbC_8 in thawing THF (ca. −100 °C) under an atmosphere of N_2. After removal of solvent and extraction with hexanes, the pure product **1-Rb** crystallized from cold hexanes in 48% yield. The *n*-hexane solvate of **1-Rb** was characterized by X-ray crystallography (Figure 1), ^{1}H NMR spectroscopy (Figure 2), and Mössbauer spectroscopy (Table 1, Figure S3). Its Mössbauer spectrum is analogous to the one reported for **1-K**[18] and consists of three doublets in a 2:1:1 ratio, which corresponds to two identical Fe^{3+} ions and two different Fe^{2+} ions. The isomer shifts for each iron environment in **1-K** and **1-Rb** are within 0.02 mm/s, and quadrupole splittings are within 0.13 mm/s (Table 1). Thus, the electronic structures of the iron sites are very similar between the two.

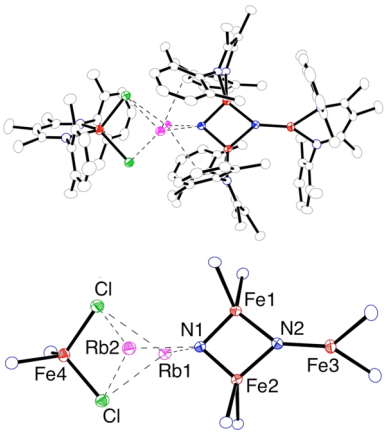

Figure 1. Thermal-ellipsoid plot (50%) of **1-Rb** (full view, top; core, bottom). Hydrogen atoms are omitted for clarity. Selected bond distances (Å) and angles (deg): Fe(1)−N(1), 1.810(2); Fe(1)−N(2), 1.908(2); Fe(2)−N(1), 1.817(2); Fe(2)−N(2), 1.926(2); Fe(3)−N(2), 1.838(2); Rb(1)−N(1), 2.825(2); Rb(2)−N(1), 2.872(2); N(1)−Fe(1)−N(2), 97.64(10); N(1)−Fe(2)−N(2), 96.75(9).

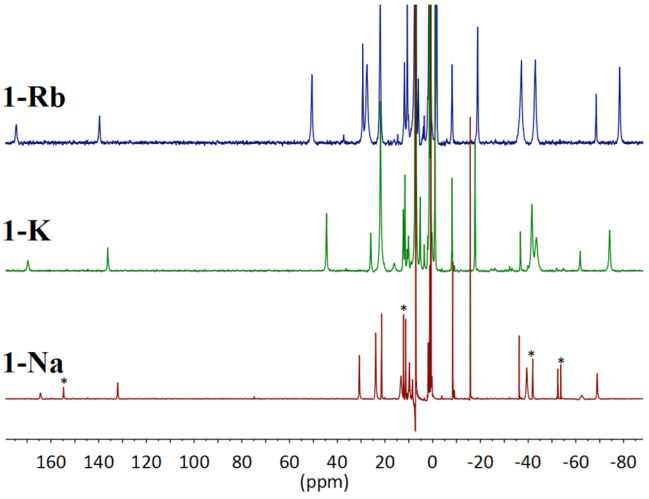

Figure 2. Comparison of the ^{1}H NMR spectra of **1-Rb** (top), **1-K** (middle), and **1-Na** (bottom) recorded in C_6D_6. Asterisks (*) indicate signals assigned to $[LFe(\mu\text{-}Cl)]_2$.

The crystal structure of **1-Rb** (Figure 1) displays an Fe_3N_2 core with distances and angles that are indistinguishable from those in **1-K**. The main difference is in the alkali-metal part of the molecule, where the Rb−N(1) distances are 1 Å *shorter* than the analogous K−N(1) distances (Table 1). We attribute the much shorter distance between Rb and N(1) to the longer bonds between Rb and the π-coordinated arene rings (average distance of M to centroids are 3.58 Å for **1-Rb** vs 3.42 Å for **1-K**), which push the Rb atoms closer to the nitride. In effect, the larger Rb^+ cations more completely fill the alkali-metal pockets than K^+, which may contribute to the higher stability of the Rb analogue (see below).

dx.doi.org/10.1021/ja507442b | J. Am. Chem. Soc. 2014, 136, 16807−16816

Table 1. Metrical and Spectroscopic Parameters for Compounds 1

	1-Na	1-K[a]	1-Rb
Fe(1)–N(1) (Å)	1.74(1)	1.812(2)	1.810(2)
Fe(2)–N(1) (Å)	1.82(1)	1.809(2)	1.817(2)
Fe(1)–N(1)–Fe(2) (deg)	85.8(6)	85.27(8)	85.6(1)
Fe(1)–N(2)–Fe(2) (deg)	81.5(5)	79.79(7)	80.00(9)
M(1)–M(2) (Å)	N/A	3.8811(9)	4.1029(5)
N(1)–M(1) (Å)	2.28(1)	3.8212(6)	2.825(2)
N(1)–M(2) (Å)	N/A	4.0017(6)	2.872(2)
Two hs Fe^{3+} (Fe1, 2)			
δ (mm/s)	0.33	0.29	0.31
$\lvert\Delta E_Q\rvert$ (mm/s)	1.56	1.79	1.87
Trig planar hs Fe^{2+} (Fe3)			
δ (mm/s)	0.74	0.68	0.66
$\lvert\Delta E_Q\rvert$ (mm/s)	1.20	1.54	1.67
Tetrahedral hs Fe^{2+} (Fe4)			
δ (mm/s)	0.96[b]	0.96	0.96
$\lvert\Delta E_Q\rvert$ (mm/s)	2.29[b]	1.80	1.91

[a]Ref 18. [b]Based on similarity of shifts and quadrupole splitting, we assign the tetrahedral hs Fe^{2+} signals to the starting material $[LFe(\mu\text{-}Cl)]_2$.

The number and integration of signals in the ^{1}H NMR spectrum of **1-Rb** (Figure 2) suggest idealized C_{2v} symmetry in the four-iron cluster, which agrees with the solid state crystal structure. Since both **1-K** and **1-Rb** are soluble in hexane, and their ^{1}H NMR spectra in C_6D_{12} and C_6D_6 solutions possess the number of peaks that are consistent with the crystal structures, it is likely that in hydrocarbon solvents the $Fe_4(K/Rb)_2N_2Cl_2$ cores remain intact. In addition, the chemical shifts of **1-Rb** are similar to those in **1-K**,[18] which for paramagnetic molecules implies similar anisotropy in the magnetic moments of the Fe ions, and a similar electronic structure.[23]

Monitoring C_6D_6 solutions by ^{1}H NMR spectroscopy shows that **1-K** (8.1 mM) and **1-Rb** (either 12.1 mM or 6.3 mM) slowly degrade at room temperature, with **1-Rb** ($t_{1/2}$ = 21 h) decomposing more slowly than **1-K** ($t_{1/2}$ = 8 h).[18] ^{1}H NMR spectroscopy shows that the primary iron-containing compounds after decomposition are the known iron(I) complex $LFe(C_6D_6)$[24] and the previously unreported iron(II) complex L_2Fe (**2**). Compound **2** is a pseudotetrahedral iron(II) complex, and its X-ray crystal structure and characterization are presented in the Supporting Information (Figure S1).

At first, formation of the iron(I) product $LFe(C_6D_6)$ from reaction of benzene with the diiron(II)diiron(III) starting materials **1-Rb** and **1-K** might seem surprising. However, in a recent paper we described reactions of **1-K** with CO, isocyanides, and benzene, which each gave iron(I) products $LFe(CO)_3$, LFe(CNXyl), and $LFe(C_6H_6)$ where the reducing equivalents come from N^{3-} oxidation.[24] In the cited work, the rate of reaction decreased in order of increasing cone angle of the attacking reagent, with slim CO and isocyanides giving rapid reactions, and benzene a substantially slower reaction. No intermediates are observed during any of these reactions. Assuming that the degradation reactions have the same initial steps, this trend suggests that the decomposition in benzene involves association of the benzene molecule with **1** in the transition state. This model rationalizes the higher stability of **1-Rb**, where the better fit of Rb^+ into the pockets in the tetrairon structure holds the core together and slows benzene attack. Further studies will be necessary to determine at what site in the molecule the benzene attacks **1-K** and **1-Rb**.

In attempt to better understand the strength of association of K^+ and Rb^+ in the bis-nitride structures in solution, we reacted solutions of **1-K** and **1-Rb** in THF with the trifluoromethanesulfonate salts KOTf and RbOTf.[25] Addition of KOTf to **1-Rb** or RbOTf to **1-K** (either 2 or 20 equiv) gives product mixtures in which the alkali metal cations are partially or completely exchanged, though there was also substantial decomposition to unknown byproducts (Figures S9, S10). It was not possible to determine equilibrium constants, because of overlap of peaks in the ^{1}H NMR spectra, formation of byproducts, and the low solubility of the alkali metal triflates.[26] With these caveats, we note that **1-K** is completely consumed after reaction with 2 equiv of RbOTf (Figure S9), suggesting a favorable equilibrium constant. Conversely, when **1-Rb** was treated with 2 equiv of KOTf, a significant amount of **1-Rb** remained (Figure S10). Addition of 20 equiv of KOTf was necessary to deplete **1-Rb** and form a significant amount of **1-K**. This suggests that **1-Rb** is more stable than **1-K**, in agreement with the slower decomposition of **1-Rb**.

N_2 Cleavage Using Sodium Yields a New Fe_3N_2 Structure. Because of the known difficulty of intercalating Na into graphite,[27] we explored other methods to reduce $[LFe(\mu\text{-}Cl)]_2$ with Na. Addition of sodium amalgam to a THF solution of $[LFe(\mu\text{-}Cl)]_2$ did not reduce the iron(II) starting material (Figure S15).[28] As an alternative, we sonicated a mixture of $[LFe(\mu\text{-}Cl)]_2$ and metallic Na in THF at 0 °C for 1 h, which led to a triiron complex, **1-Na** (Figure 3), in 48% yield. To compare this synthetic method to the one used for obtaining **1-K** (reduction by KC_8), we also sonicated metallic K in THF at 0 °C for 1 h. ^{1}H NMR spectra of the crude reaction mixture (Figure S17) showed **1-K** as the major species, and thus the product does not seem to be influenced by the use of powdered metal vs the graphite complex. This indicates that differences in the product structures can be attributed to the change in the alkali metal, rather than the preparation method.

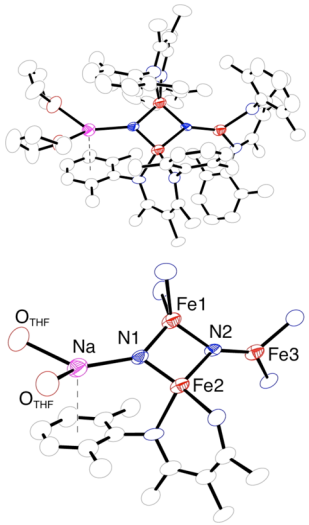

Figure 3. Thermal-ellipsoid plots (50%) of **1-Na** (top) and its core (bottom). Hydrogen atoms were omitted for clarity. Selected bond distances (Å) and angles (deg): Fe(1)–N(1), 1.74(1); Fe(1)–N(2), 1.88(1); Fe(2)–N(1), 1.82(1); Fe(2)–N(2), 1.84(1); Fe(3)–N(2), 1.81(1); Na(1)–N(1), 2.825(2); N(1)–Fe(1)–N(2), 96.9(6); N(1)–Fe(2)–N(2), 95.7(6).

dx.doi.org/10.1021/ja507442b | J. Am. Chem. Soc. 2014, 136, 16807–16816

The X-ray crystal structure of **1-Na** has a relatively high *R* value of 8.2%, mostly from explicit inclusion of a *n*-hexane solvent molecule and disorder in a xylyl group; this gave relatively large esd values, but did not influence the assignment of the core structure of the molecule. **1-Na** is different from **1-K** and **1-Rb** because it lacks the fourth, tetrahedral Fe atom and has only one alkali metal cation; the coordination at sodium is completed by two THF molecules. The Na−N(1) distance is 1.5 Å shorter than the K−N(1) distance in **1-K** and 0.5 Å shorter than the Rb−N(1) distance in **1-Rb** (Table 1). The Na-centroid distance is also shorter at 2.745(7) Å. The Fe_3N_2 core in **1-Na** is more symmetric than that in **1-K** and **1-Rb** (Table 1, Figure S2), and the oxidation states of iron centers may be assigned as two equivalent Fe^{3+} sites (Fe1 and Fe2) and one Fe^{2+} site (Fe3) based on the overall charge count and the similarity of the Mössbauer parameters to the analogous positions in **1-K** and **1-Rb** (Table 1, Figure S4).

During formation of **1-Na**, there is an apparent imbalance between the reduction ($6e^-$ reduction of N_2) and oxidation ($5e^-$ oxidation of 3 Fe) half-reactions. However, **1-Na** is not the only species that exists in the reaction mixture. One of the most prominent byproducts is $[LFe(\mu\text{-}Cl)]_2$, which is difficult to separate and thus is present in amounts up to 0.89 mol per mol of **1-Na**. This iron(II) chloride dimer was identified by comparison of its ^{1}H NMR and Mössbauer parameters to the known compound.[18] We propose that the sixth electron for N_2 reduction comes from an unidentified Fe^{1+} species that (like the fourth Fe in **1-K** and **1-Rb**) is oxidized to an iron(II) chloride product; however, the Na^+ cation fits so poorly into the K/Rb position of the tetranuclear structure that this iron(II) chloride does not bind in an analogous fashion. Rather, in the Na system the iron(II) chloride species dissociates and dimerizes to $[LFe(\mu\text{-}Cl)]_2$. The heterogeneous nature of the reaction has prevented us from exploring this hypothesis in greater mechanistic detail.

Interestingly, the thermal stability of **1-Na** in C_6D_6 solution ($t_{1/2}$ = 35 h) is greater than its **1-K** and **1-Rb** analogues, which does not fit the trend of greater stability of heavier **1-Rb** over **1-K**. We propose that the reaction of **1-Na** with benzene is slower because the mechanism is different; after all, there are not enough Fe sites to accept the six electrons from two N^{3-} to reform N_2 in the mechanism followed by **1-K** and **1-Rb**.[24] The ^{1}H NMR spectra after decomposition of **1-Na** (Figure S16) similarly show significant formation of $LFe(C_6D_6)$, which requires an external oxidant to accept the sixth electron. However, the decomposition mixture from **1-Na** is complicated, and substantial amounts of **2** and $[LFe(\mu\text{-}Cl)]_2$ are also observed.

In order to test the ability to exchange the cations in the different bis-nitride structures, we treated **1-Na** (which contained some $[LFe(\mu\text{-}Cl)]_2$, as noted above) with KOTf and RbOTf (20 equiv) in THF, and analyzed the products using ^{1}H NMR spectroscopy (Figures S11−S14). As with the K^+-Rb^+ exchange reactions described above, the product mixtures had substantial amounts of unidentified decomposition products, but the characteristic ^{1}H NMR resonances of **1-K** and **1-Rb** were present. Interestingly, the addition of even this large excess of KOTf gave a mixture containing residual **1-Na**, which supports the idea that **1-K** is less stable than **1-Na**. We also treated **1-K** and **1-Rb** with 20 equiv of NaOTf, which entirely consumed the starting materials and gave **1-Na** as a major product. These support the idea that **1-Na** has greater inherent stability, though the concurrent formation of $[LFe(\mu\text{-}Cl)]_2$ complicates any thermodyamic analysis.

We have also attempted to synthesize the Li analogue of complexes **1**, using the sonication method described above for **1-Na**. However, we have observed that even before the beginning of reaction, Li metal tarnished upon exposure to N_2 atmosphere. This result is not surprising, as it is known that Li^0 reacts with N_2 to yield Li_3N.[29] Even though a brief formation of a new complex can be observed by ^{1}H NMR spectroscopy, we were unable to isolate this new species, even by low-temperature crystallization. ^{1}H NMR analysis of the post-crystallization mixture showed the presence of $[LFe(\mu\text{-}Cl)]_2$, LFe(Cl)(THF), and **2**. Therefore, we surmise that the Li analogue of complexes **1** is very unstable.

Triiron Cores with N_2 Bridges. Reduction of $[LFe(\mu\text{-}Cl)]_2$ with 2 equiv of cesium graphite (CsC_8) did not yield the Cs analogue of **1-K**, but instead gave a trinuclear complex **3-Cs** with two N_2 units bound in an end-on/end-on mode (Figure 4). This compound has not been obtained in pure form. The presence of one Cl^- bridge in the structure suggested incomplete reduction of the starting material.

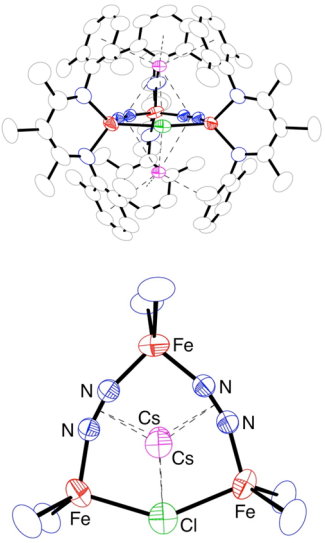

Figure 4. Thermal-ellipsoid plots (50%) of **3-Cs**, from two views. Hydrogen atoms omitted for clarity. **3-Cs** has crystallographic D_3 symmetry imposed on each molecule, with disorder between two N_2 and one Cl bridge. One chemically reasonable disorder component is shown. Selected bond distances (Å) and angles (deg): Fe−N(N_2), 1.829(5); Fe−Cl(1), 2.505(3); N(N_2)−N(N_2), 1.234(11); Fe−N(diket), 1.979(3); N(N_2)−Fe(1)−N(N_2), 95.7(5), N(N_2)−Fe(1)−Cl, 97.6(3), Fe−Cl−Fe, 140.5(4).

Addition of further equivalents of CsC_8 to samples of **3-Cs** did not give further N_2 incorporation or reduction. This result, and the presence of chloride in **3-Cs**, prompted us to add 4 equiv of CsC_8 per $[LFe(\mu\text{-}Cl)]_2$ in a single step, which gave a new class of Fe−N_2 complex. Interestingly, the use of 4 equiv of RbC_8 or KC_8 gave products with very similar ^{1}H NMR spectra. The blue-green products were identified as $M_2[LFe(\mu\text{-}N_2)]_3$ (**4-K**, **4-Rb**, **4-Cs**) through X-ray crystallography of the Rb and Cs species (Figures 5 and S24).

The cesium compound **4-Cs** was the most stable of these triangular complexes, and it was isolated in 86% yield, while **4-Rb** was isolated in a lower yield of 69%. These molecules were not stable under a vacuum, as shown by cracking of crystals.

dx.doi.org/10.1021/ja507442b | J. Am. Chem. Soc. 2014, 136, 16807−16816

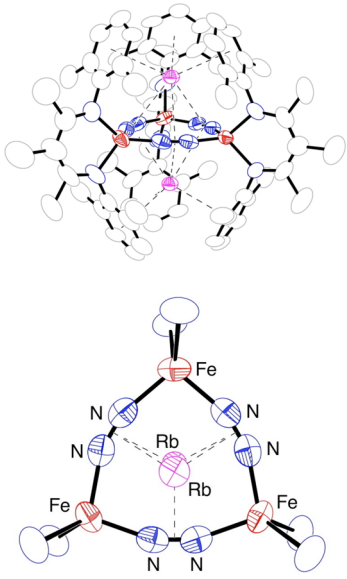

Figure 5. Thermal-ellipsoid plots (50%) of **4-Rb**. The Cs analogue (**4-Cs**) is shown in Figure S24 (Supporting Information). Both molecules have crystallographic D_3 symmetry. Hydrogen atoms are omitted for clarity. Selected bond distances (Å) and angles (deg): Fe(1)−N(N_2), 1.839(7); N(N_2)−N(N_2), 1.191(14); Fe(1)−N(diket), 1.971(8); N(N_2)−Fe(1)−N(N_2), 99.3(5).

Further, the microanalytical results were systematically low in nitrogen, suggesting that N_2 can be released from the structure; Mössbauer spectroscopy also showed presence of secondary doublets (see Figures S6 and S7). Despite these problems, the ^{1}H NMR spectrum in C_6D_6 (Figure 6) indicated high purity,

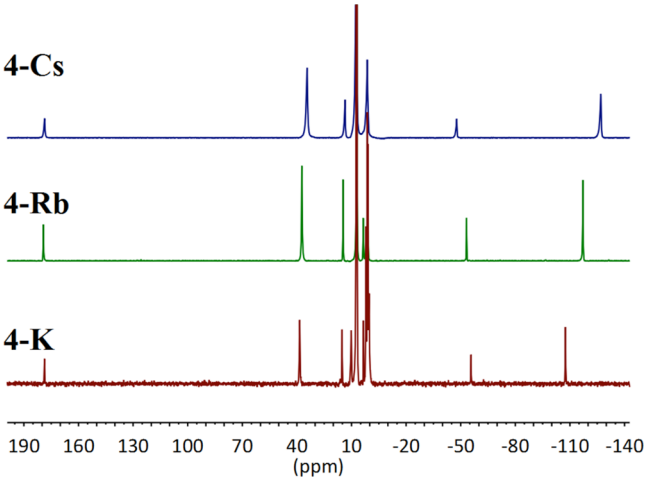

Figure 6. Comparison of the ^{1}H NMR spectra of **4-Cs** (top), **4-Rb** (middle), and **4-K** (bottom) in C_6D_6.

suggesting that the changes are reversible. The ^{133}Cs NMR spectrum of **4-Cs** in C_6D_6 showed a single broad peak with fwhm = 226 Hz (Figure S18). The broadness is attributed to rapid relaxation of the Cs nuclear spin by the nearby paramagnetic Fe centers. There are no other peaks in the spectrum corresponding to Cs-containing impurities.[30]

The isostructural triiron compounds **4-Rb** (Figure 5) and **4-Cs** (Figure S24) have interesting triangular $Fe_3(\mu\text{-}N_2)_3$ cores. Crystallographic C_2 and C_3 axes enforce D_3 point group symmetry that makes all three Fe atoms and all six nitrogen

Table 2. Mössbauer and Metrical Parameters of Complexes 4

	4-K	4-Rb	4-Cs
δ (mm/s)	0.68	0.71	0.74
$\lvert\Delta E_Q\rvert$ (mm/s)	0.67	0.58	0.47
Fe−N_{N2} (Å)	–	1.839(6)	1.841(4)
N−N (Å)	–	1.191(14)	1.199(7)

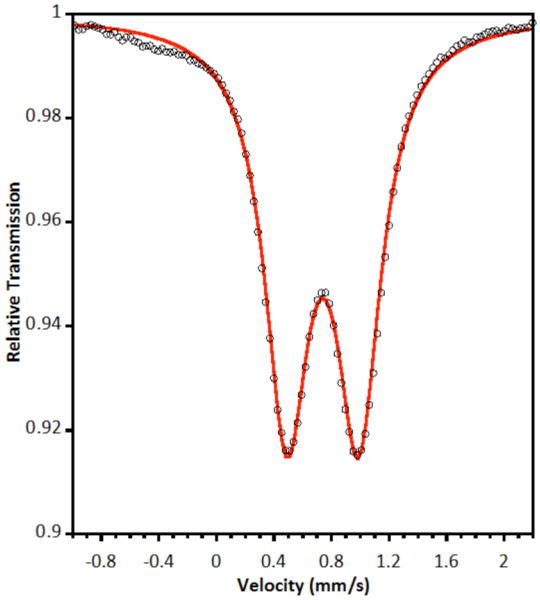

Figure 7. Zero-field Mössbauer spectrum of **4-Cs** recorded at 80 K. The black circles represent the data, and the red line is the fit to parameters given in Table 2. Spectra of **4-K** and **4-Rb** are given in the Supporting Information (Figures S5, S6).

atoms of the N_2 bridges equivalent. The N−N distances in the N_2 bridges are indistinguishable at 1.191(14) Å (**4-Rb**) and 1.200(9) Å (**4-Cs**). This extent of N−N lengthening is similar to that observed previously in linear Fe(μ-N_2)Fe cores of larger diketiminate ligands, and suggests partial reduction of N_2.[16] The solid-state Mössbauer spectra of **4-Rb** and **4-Cs** at 80 K each show a quadrupole doublet with δ ~0.7 mm/s and $\lvert\Delta E_Q\rvert$ ~0.5 mm/s (Table 2). The isomer shifts are similar to that in $L^{Me,iPr}FeNNFeL^{Me,iPr}$ ($L^{Me,iPr}$ = 2,4-bis(2,6-diisopropylphenylimino)pent-3-yl, δ = 0.62 mm/s).[31] Figure 7 shows the Mössbauer spectrum of **4-Cs**, and the parameters used to obtain this fit are given in Figure S7. The observation of only one doublet in the Mössbauer spectrum of this mixed-valent compound indicates that the valence is delocalized over the entire core on the Mössbauer time scale (~10^{-9} s) at 80 K. Detailed studies on the electronic structure and magnetism of compounds **4** will be reported separately.

Each of the triiron compounds **4** has a planar $Fe_3(\mu\text{-}N_2)_3$ core, with Fe−N distances of 1.839−1.841 Å, and N−Fe−N angles of 97−99°. The planar Fe_3N_6 core is capped on each face by an alkali metal, and the M-M distances between the alkali metals are similar (Rb−Rb = 5.017(3) Å; Cs−Cs = 5.172(2) Å). The distances between the alkali metals and the arene centroids are similar at 3.2980(8) and 3.3162(6) Å, respectively. Since the compounds are soluble in aromatic hydrocarbons, we infer that in solution the alkali metals remain coordinated, to give uncharged compounds in which cations are shielded from the external solvent by the surrounding xylyl arms. This assessment is also corroborated by ^{1}H NMR

dx.doi.org/10.1021/ja507442b | J. Am. Chem. Soc. 2014, 136, 16807−16816

spectroscopy, where the number of peaks points to a D_{3h} averaged structure in solution (Figure 6). However, the Mössbauer spectrum of a frozen THF solution of **4-Cs** had a second, smaller doublet at δ = 0.37 mm/s and $|\Delta E_Q|$ = 1.10 mm/s that was not present in the solid sample. Considering the low N analysis, we attribute the second doublet to a solution species where THF has coordinated to one or more iron centers and/or replaced one or more N_2 units. Beer's Law plots of **4-Cs** in THF (Figure S23) was nonlinear, corroborating the idea that the behavior in THF is complicated.[32]

We were unable to obtain a single crystal of **4-K**, which had lower thermal stability than its Rb and Cs analogues. Though it was not sufficiently pure for elemental analysis, it was isolated as a powder in 29% yield. The structure of **4-K** is likely to be analogous to its Rb and Cs analogues based on the similarity of its solution ^{1}H NMR (Figure 6) and solid-state Mössbauer (Figure S5) parameters to **4-Rb** and **4-Cs**. We propose that the lower stability of **4-K** is a result of the smaller cation: only the Rb^+ and Cs^+ cations are large enough to form sufficiently stable cation-π interactions with all three xylyl appendages.

Reactions with Acid to Give Ammonia. We have previously reported that diketiminate-supported Fe complexes with bridging Fe-NN-Fe cores do not form any ammonia upon addition of acid, whether at the formal Fe^{1+} or Fe^0 oxidation level.[16] Consistent with this trend, treatment of the bridging N_2 complexes **4-Rb** or **4-Cs** with excess HCl gave no detectable ammonia, as measured using the indophenol test.[33] In contrast, **1-K** has two nitrides that can be protonated with anhydrous HCl to release the two nitrides as ammonia in a yield of 80 ± 4%.[18] Under the same conditions, **1-Rb** reacted with an excess of anhydrous HCl to give a 73 ± 1% yield of ammonia, and **1-Na** released ammonia in a quantitative (99 ± 2%) yield. We attribute the higher yield for **1-Na** to its hindered ability to reform the N−N bond to produce N_2 as found for **1-K**,[24] on account of its different structure and inability to accept more than five electrons (see above).

DISCUSSION

Novel Fe−N_2 Compounds from Alkali-Metal Reduction of Iron(II) Chloride Complexes under N_2. The above results show that K is not unique in its ability to facilitate N_2 reduction by Fe in the iron(I) oxidation level. Na and Rb also promote complete six-electron reduction of N_2, and form compounds with analogous trinuclear $Fe^{3+}{}_2Fe^{2+}(N)_2$ cores (**1**) where the two nitrides are derived from N−N bond scission. It is evident that the size of the alkali-metal cations influences the structure and stability of the N_2-cleaved complexes **1**, with the larger cation Rb^+ resulting in higher stability than K^+. This trend is opposite of the one for the gas phase cation-π interactions, which are strongest for the lighter alkali metals.[34] M−N bond strengths are expected to follow a similar trend. Thus, it is likely that the stability is determined by the ability of the cation to fit into a cavity of the appropriate size, where the fit in the tetranuclear $L_4Fe_4M_2Cl_2$ structure is more ideal for Rb^+ than K^+.

On the basis of these considerations, we propose that Na^+ fits so poorly into the tetranuclear structure that it forms the different trinuclear structure in **1-Na**. Within this structure the "dangling" Fe−Cl is absent, and the Na^+ ion completes its coordination with THF molecules instead of bridging chlorides. Though the structure is different, addition of K^+ or Rb^+ salts to mixtures of **1-Na** and $[LFe(\mu\text{-Cl})]_2$ gives **1-K** and **1-Rb**, and vice versa. These metathesis reactions favor formation of **1-Na**, which may be more thermally stable, but these reactions are accompanied by some decomposition that limits the ability to assess the thermodynamics of the system. Future studies will explore the reactivity of these cores and the possibility to remove the alkali metals completely.

This Article also reports a new kind of triangular metal-dinitrogen core (**4**) derived from three iron atoms and three end-on/end-on bridged N_2 units. This shape of metal-dinitrogen complex has not been reported in any literature metal-N_2 compounds, with the exception of a Re compound that was deposited in the CSD as a personal communication.[35] Part of the stability of the $Fe_3(\mu\text{-}N_2)_3$ core undoubtedly arises from cation-π interactions between the alkali metal cation and the three nearby arene rings of the supporting ligands. The stability of the compounds in solution changes in the order $Cs^+ > Rb^+ > K^+$, which is consistent with the larger cation being able to more easily coordinate to three arene rings without steric destabilization.

More Reduction Gives Less N_2 Activation. Reduction of the Fe^{2+} compound $[LFe(\mu\text{-Cl})]_2$ by 1e^- per Fe leads to N_2 cleavage to nitrides (**1**), which react with HCl to give high yields of ammonia. However, reduction by 2e^- per Fe gives N_2 complexes (**4**) that neither cleave the N−N bond nor produce ammonia when treated with acid. Clearly, it is not the *number* of reducing equivalents present that determines the extent of N−N activation. Additionally, because we use graphite-supported alkali metals where the reducing electrons are on the graphite, the *reducing power* of the reductant is unlikely to vary significantly between the different alkali-metal reductants.

We propose that instead, the observed differences in the ability to reduce N_2 can be explained by considering the *geometry* of the multimetallic iron-alkali-N_2 species that are accessible at each reduction level.[14] As shown in a recent computational paper, three neutral LFe^{1+} fragments are sufficient to cooperatively weaken and cleave the N−N bond of N_2, with the participation of a K^+ ion.[36] The key postulated intermediate derived from the computations is shown in Figure 8, and it can form when three iron atoms simultaneously approach N_2. We propose that this cooperative interaction is not possible when over-reduction gives species like **4**, in which the cation-π interactions enforce an expanded core size that prevents three Fe atoms from approaching one another closely. In the shape of the triangular clusters **4**, no more than two iron atoms can reach a single molecule of N_2 at the same time, and N_2 cleavage is not observed.

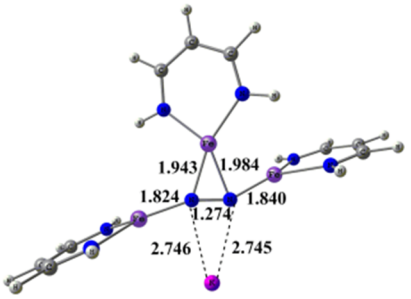

Figure 8. Calculated structure for a potential N_2 reduction intermediate, indicating how three LFe units could interact with N_2.[36]

Thus, we propose that the key factor in the iron-mediated N−N bond scission is the number of Fe atoms that attack the N_2 unit simultaneously, and that the shape of the structure

dx.doi.org/10.1021/ja507442b | J. Am. Chem. Soc. 2014, 136, 16807−16816

enforced by the cation-π interactions to the alkali metal cations is more important than the oxidation level of the iron atoms. This idea also explains the inability of iron complexes with larger diketiminate ligands to cleave the N−N bond,[16] because they form protected FeNNFe cores where the supporting ligand blocks approach of a third iron atom. Further support for these ideas will require isolation of intermediates, and/or computations that model more of the cluster environment.

It is interesting to compare these alkali cation linked diketiminate supporting ligands to the covalently linked cyclophane-diketiminate supporting ligands reported recently by Murray and co-workers, which can support three preorganized Mn, Fe, or Cu ions.[37,38] There is a clear analogy between the triiron cores accessed here and the trimetallic cores that come from these diketiminate-cyclophane ligands. The covalent linkages in the cyclophane-diketiminate ligands are stronger and more rigid, which lends predictability and may enforce N_2 binding in $Cu_3(\mu\text{-}\eta^1{:}\eta^2{:}\eta^1\text{-}N_2)$, the first example of any isolated copper-N_2 complex.[38] The cation-π interactions in the complexes described here are weaker, more labile, and more difficult to predict. On the other hand, the flexibility of the cation-π interactions is advantageous for the serendipitous discovery of unforeseen core structures. Another advantage is that the ease of varying alkali metals enables one to tune the structure and reactivity of the alkali metal complexes rapidly without the need to synthesize new supporting ligands. Thus, each method has different advantages.

CONCLUSIONS

Diketiminate ligands can support a number of novel Fe−N_2 complexes, including some containing a novel triangular N_2-bridged trimetallic core, and others that are able to perform the six-electron reduction of N_2 to nitrides. We have also addressed the influence of the identity of the alkali metal on N−N bond scission in multiiron complexes. Our model, in which cooperation between three Fe atoms and N_2 is necessary for N−N bond scission, explains the need for relatively small diketiminate supporting ligands to enable close Fe−Fe distances during the critical step.[39] Overall, our results support the idea that alkali metals can steer three iron atoms to cooperatively cleave the N−N bond, whereas N−N cleavage does not take place when only two Fe atoms can approach N_2. This observation has implications for the Haber−Bosch catalyst, where K-promoted triiron sites should be considered as key potential sites for N−N cleavage. Additionally, we propose that alkali metals could bind to nitrides resulting from N−N scission. We recommend that future studies test these ideas for the surface catalysts.

EXPERIMENTAL SECTION

General Methods. All manipulations were performed in an MBraun glovebox in an N_2 atmosphere maintained at or below 1 ppm of O_2. All glassware was oven-dried at 150 °C for at least 12 h before use. Pentane, hexanes, diethyl ether, and toluene were purified by passage through activated alumina and "deoxygenizer" columns (Glass Contour Co., Laguna Beach, CA). Tetrahydrofuran (THF) was dried by distilling from Na/benzophenone. All solvents were stored over activated 3 Å molecular sieves and passed through a plug of activated alumina before use. Deuterated benzene was dried over activated alumina and then filtered before use. THF-d_8 was dried over CaH_2 and then over Na^0/benzophenone, and vacuum transferred to a storage container before use. Graphite, Celite, and 3 Å molecular sieves were dried at 300 °C under a vacuum for >12 h.

^{1}H NMR spectra were recorded on either an Avance 400, Avance 500, or Agilent 500 spectrometer, and are referenced to residual C_6D_5H at δ 7.16 ppm. UV−vis spectra were recorded on a Cary 50 spectrometer using Schlenk-adapted quartz cuvettes with a 1 mm path length. IR spectra were recorded as KBr pellets on a Shimadzu 8400S FTIR, or as solids in ATR mode on a Bruker Alpha FTIR. Elemental analysis data were obtained from the CENTC Elemental Analysis Facility at the University of Rochester. The indophenol test for NH_3 quantification was performed as previously described.[33] Quantification of the amount of **1-Na** for the indophenol procedures was performed using relative integration of the most downfield shifted peaks, which are assigned as 3 H in case of both $[LFe(\mu\text{-}Cl)]_2$ and **1-Na**.

Benzylpotassium was synthesized using the published method.[40] $FeCl_2(THF)_{1.5}$[41] and ligand HL[18] were synthesized using previously published procedures. Rubidium trifluoromethanesulfonate was prepared according to the literature procedure.[42] Potassium trifluoromethanesulfonate was purchased from Sigma-Aldrich and dried under a vacuum (0.2 mTorr) for 24 h at 160 °C. Metals were obtained from the following vendors: lithium from ACROS (99+%, granular, dry), sodium from TJ Baker (Baker analyzed Na lump); potassium (98% pure) from Sigma-Aldrich; rubidium from Alfa Aesar (99.75% pure); cesium from Strem (99.9% pure). Potassium graphite (KC_8) was prepared by heating stoichiometric amounts of potassium and graphite at 145 °C under an argon atmosphere. Rubidium graphite (RbC_8) was prepared by heating stoichiometric amounts of rubidium and graphite at 130 °C under an argon atmosphere. Cesium graphite (CsC_8) was prepared by mixing stoichiometric amounts of cesium and graphite at ambient temperature under argon atmosphere.[43] ***Warning:*** *Alkali metals and their graphite intercalates KC_8, RbC_8, and CsC_8 are powerful reductants, which ignite on contact with air and moisture. Therefore, extreme care must be taken when synthesizing and handling these alkali graphite reductants!*

$[LFe(\mu\text{-}Cl)]_2$. $[LFe(\mu\text{-}Cl)]_2$ was synthesized by a variant of the previously published procedure.[18] In the glovebox, benzylpotassium (1.77 g, 14.0 mmol) was dissolved in 40 mL of THF and added to a rapidly stirring solution of HL (4.34 g, 14.0 mmol) in THF (10 mL) at ambient temperature. The reaction was stirred for 40 min until a uniform bright-yellow color was observed, indicating the formation of KL. At this point, the solution was cooled in the cold well below −78 °C. $FeCl_2(THF)_{1.5}$ (3.18 g, 14.0 mmol) was suspended in 100 mL of THF and cooled in the cold well below −78 °C. Next, the cold solution of KL was added very slowly to a rapidly stirring suspension of $FeCl_2$ over 5 min and allowed to warm to ambient temperature while stirring for 12 h. The dark brown-yellow-green suspension was then dried for >8 h under a vacuum (0.020 Torr) at 40 °C. The solid was then suspended in 60 mL of toluene, heated to reflux under N_2 for 1 h, and filtered through Celite while still hot. The solvent was removed from the filtrate under a vacuum, and the red-orange solid was washed with pentanes until the wash was colorless (3 × 15 mL). The yield of red-orange solid was 4.36 g (80%). The ^{1}H NMR shifts match those reported previously.[18] (500 MHz, C_6D_6): δ 155 (3H, α-methyl), 12.2 (4H, *m*-aryl), 9.8 (12H, *o*-methyl), −42.0 (6H, β-methyl), −53.7 (2H, *p*-aryl) ppm.

$[THF]_2(Na)[LFe]_2(\mu_2\text{-}N)(\mu_3\text{-}N)[FeL]$ (1-Na). In an N_2-filled glovebox, a piece of metallic sodium (5.7 mg, 0.248 mmol) was deposited on a bottom of a 250 mL bomb flask, covered with THF (∼1.5 mL), and frozen. In a separate scintillation vial, $[LFe(\mu\text{-}Cl)]_2$ (87.0 mg, 0.108 mmol) was dissolved in THF (2 mL), cooled to the freezing point, and slowly added to the bomb flask, making sure that it froze on the glass walls. The flask was then taken out of the box and sonicated for 1 h at 0 °C. Next, the bomb flask was taken back into the box, where solvent was removed under reduced pressure. The resulting dark green solid was suspended in hexanes (∼5 mL) and filtered through Celite. The red filtrate was concentrated to ∼1 mL and cooled to −40 °C for 3 h to give dark red crystals (48.2 mg, 48%). This material is typically impure, with 10−30 mol % $[LFe(\mu\text{-}Cl)]_2$ cocrystallized. We were unable to separate these completely, so the yield above was calculated by correcting the mass for the impurity using the ratio of peaks found by ^{1}H NMR spectroscopy. ^{1}H NMR (500 MHz, C_6D_6): δ 164, 132, 30.8, 23.9, 21.4, 13.2, 12.2, 11.3, −8.44,

−15.7, −36.3, −39.4, −52.5, −62.4, −68.9 ppm (peak assignments and integrations not carried out due to overlap with peaks belonging to $[LFe(\mu\text{-}Cl)]_2$).

$[LFeCl_2](Rb)_2[LFe]_2(\mu_2\text{-}N)(\mu_3\text{-}N)[FeL]\cdot 1.5$Hexane (1-Rb). In an N_2-filled glovebox, $[LFe(\mu\text{-}Cl)]_2$ (182.6 mg, 0.226 mmol) was dissolved in THF (2 mL), frozen, and then allowed to slowly thaw. The freshly thawed solution was added in one portion to cold (<−40 °C), solid RbC_8 (94.4 mg, 0.520 mmol, 2.3 equiv) and the color immediately turned deep green. The mixture was stirred at ambient temperature for 40 min. The solvent was removed under reduced pressure, and resulting solid was extracted with 5 mL of hexanes and filtered through Celite to give a dark red solution. The filtrate was concentrated to 0.5 mL and cooled to −40 °C for 3 h to give dark red crystals (111 mg, 48%). This reaction failed when the concentration of the starting material $[LFe(\mu\text{-}Cl)]_2$ was below about 0.15 mM. ^{1}H NMR (500 MHz, C_6D_6): δ 175 (3H), 140 (3H), 50.6 (6H), 29.3/27.6 (18H), 22.0 (12H), 11.8/10.6 (12H), 6.00 (4H), 1.24/0.88 (hexane), −1.62 (18H), −8.14 (4H), −18.8 (8H), −37.2 (14H), −43.0 (12H), −68.5 (2H), −78.4 (6H) ppm. Anal. Calcd for $C_{94}H_{122}Cl_2Fe_4N_{10}Rb_2\cdot 1.5C_6H_{12}$: C, 62.37, H, 7.11, N, 7.06. Found: C, 62.62, H, 6.94, N, 7.41. IR (significant bands; KBr, cm^{-1}): 2952 (s), 2917 (s), 2856 (s), 1530 (s), 1464 (s), 1410 (s), 1346 (vs), 1290 (m), 1195 (vs), 1090 (m), 990 (s), 801 (m), 764 (vs). μ_{eff} = 7.50 ± 0.03 μ_B.

$Cs_2[LFe(\mu\text{-}Cl)(\mu\text{-}N_2)_2]$ (3-Cs). In an N_2-filled glovebox, complex $[LFe(\mu\text{-}Cl)]_2$, (33.6 mg; 0.042 mmol) was dissolved in THF (2 mL) and frozen. Upon thawing, this canary yellow solution was added to a cold (<−40 °C) solid CsC_8 (21.9 mg; 0.096 mmol), resulting in a dark green-blue suspension. This suspension was stirred for 30 min at ambient temperature. After this time solvent was removed under reduced pressure and obtained solid was suspended in hexanes (40 mL) and filtered through Celite. The solution was concentrated to ∼1 mL under reduced pressure. The solution was cooled to −40 °C to give crystals. Crystals of this compound were obtained from a mixture and cocrystallized with complex **4-Cs**, therefore ^{1}H NMR shifts (ppm) and their assignments are somewhat ambiguous. The spectrum is shown in Figure S19.

$K_2[LFe(\mu\text{-}N_2)]_3$ (4-K). In an N_2-filled glovebox, $[LFe(\mu\text{-}Cl)]_2$ (71.1 mg, 0.088 mmol) was dissolved in THF (2 mL) and frozen. Upon thawing, it was added to a cold (<−40 °C) flask containing solid KC_8 (50.0 mg; 0.370 mmol) and the mixture immediately turned dark green. The resulting suspension was stirred for 20 min at ambient temperature. The solvent was then removed under reduced pressure, and the resulting solid was suspended in 20 mL of pentane and filtered through Celite. The solvent was removed under reduced pressure and the resulting solid was washed once with cold (<−40 °C) hexanes (1 mL). After drying under a vacuum for 15 min, a dark blue-green solid was collected (22.0 mg, 29%). ^{1}H NMR (500 MHz, C_6D_6): δ 178.5 (3H; α-Me), 34.3 (12H, *o*-Me), 15.2 (4H, *m*-Me), −55.6 (2H, *p*-Me), −107.4 (6H, β-Me) ppm. Drying led to apparent loss of N_2, as evidenced by results of elemental analysis, where low N numbers were dependent on the amount of time complex spent being dried under a vacuum (see Supporting Information).

$Rb_2[LFe(\mu\text{-}N_2)]_3$ (4-Rb). In an N_2-filled glovebox, $[LFe(\mu\text{-}Cl)]_2$, (99.5 mg, 0.123 mmol) was dissolved in THF (2 mL) and frozen. Upon thawing, this canary yellow solution was added to a cold (<−40 °C) solid of RbC_8 (94.0 mg, 0.518 mmol). The mixture immediately turned dark green-blue. The suspension was stirred for 2 h at ambient temperature. After this time, THF (50 mL) was added and this diluted suspension was filtered through Celite to give a dark blue solution with a red tint. The solvent was then removed under reduced pressure and the solid was washed with cold hexanes until no red tint was observed in the wash (4 × 1 mL). The resulting solid was dried under a vacuum for 15 min (78.5 mg, 69%). Crystals for X-ray crystallography were obtained from hexanes solution at −40 °C. ^{1}H NMR (500 MHz, C_6D_6): δ 179.4 (3H, α-Me), 37.4 (12H, *o*-Me), 14.8 (4H, *m*-Me), −53.16 (2H, *p*-Me), −117.0 (6H, β-Me) ppm.

$Cs_2[LFe(\mu\text{-}N_2)]_3$ (4-Cs). In an N_2-filled glovebox, $[LFe(\mu\text{-}Cl)]_2$ (42.8 mg, 0.052 mmol) was dissolved in THF (2 mL) and frozen. Upon thawing, this canary yellow solution was added to a cold (<−40 °C) solid of CsC_8 (51.0 mg, 0.223 mmol), resulting in a dark green-blue suspension, which was then stirred for 2 h at ambient temperature. After this time, THF (50 mL) was added and this diluted suspension was filtered through Celite to give a dark blue solution with a red tint. The solvent was removed under reduced pressure and the solid was washed with cold hexanes until no red tint was observed in the wash (4 × 1 mL). The resulting solid was dried under a vacuum for 15 min (44.8 mg, 86%). Crystals for X-ray crystallography were obtained from hexanes solution at −40 °C. ^{1}H NMR (500 MHz, C_6D_6): δ 178.3 (3H, α-Me), 34.3 (12H, *o*-Me), 13.5 (4H, *m*-Me), −47.7 (2H, *p*-Me), −126.8 (6H, β−Me) ppm. UV−vis (toluene, $mM^{-1}cm^{-1}$): 330 (>42), 390 (>20), 660 (>7.5) nm; assessment of extinction coefficients is approximate, as they do not obey the Beer−Lambert Law (Figures S22 and S23).

Cation Exchange Experiments. Complex **1** was dissolved in THF (1 mL) and added to a rapidly stirring suspension of the MOTf salt in THF. After 30 min of stirring, solvent was removed under reduced pressure. The resulting red solid was suspended in hexanes (15 mL) and filtered through a Celite plug. The filtrate was then brought to dryness under a vacuum and analyzed by ^{1}H NMR spectroscopy. Reactions with excess (20 equiv) of MOTf salts were performed and analyzed in the same manner. Reactions involving **1-Na** started with mixture of **1-Na** and $[LFe(\mu\text{-}Cl)]_2$ in a 1:0.69 ratio (determined by ^{1}H NMR spectroscopy) and the amounts of trimethanesulfonate salts were calculated assuming 100% **1-Na**. The ^{1}H NMR spectra are shown in Figures S9−S14.

^{57}Fe Mössbauer Spectroscopy. Solid Mössbauer samples were packed into Delrin sample cups and loaded into the spectrometer at 77 K. Mössbauer measurements were performed using a SEE Co. MS4 Mössbauer spectrometer integrated with a Janis SVT-400T He/N_2 cryostat for measurements at 80 K with a 0.07 T applied magnetic field. Isomer shifts were determined relative to α-Fe at 298 K. All Mössbauer spectra were fit using the program WMoss (SEE Co.), using Lorentzian doublets.

X-ray Crystallography. Single crystals (except of **1-Na**) were placed onto the tip of a 0.1 mm diameter glass capillary tube or fiber and mounted on a Bruker SMART APEX II CCD Platform diffractometer for a data collection at 100.0(1) K.[44] A preliminary set of cell constants and an orientation matrix were calculated from reflections harvested from three orthogonal wedges of reciprocal space. The full data collection was carried out using Mo Kα radiation (graphite monochromator) with appropriate frame times ranging from 45−90 seconds with a detector distance of 4.00 cm. Single crystal of **1-Na** was placed onto the fiber loop and mounted on a Rigaku R-AXIS RAPID diffractometer coupled to an R-AXIS RAPID imaging plate detector with Mo Kα radiation (λ = 0.71073 Å) at 93(2) K. The structures were solved using SIR97[45] and refined using SHELXL-97 or SHELXL-2013.[46] A direct-methods solution was calculated which provided most non-hydrogen atoms from the E-map. Full-matrix least squares/difference Fourier cycles located the remaining non-hydrogen atoms. All non-hydrogen atoms were refined with anisotropic displacement parameters. All hydrogen atoms were placed in ideal positions and refined as riding atoms with relative isotropic displacement parameters. Details are given in Table S2.

■ ASSOCIATED CONTENT

Supporting Information

Additional spectroscopic and crystallographic information. This material is available free of charge via the Internet at http://pubs.acs.org.

■ AUTHOR INFORMATION

Corresponding Author

patrick.holland@yale.edu

Notes

The authors declare no competing financial interest.

■ ACKNOWLEDGMENTS

This work was supported by the National Institutes of Health (GM065313) and Yale University. Analytical data were obtained from the CENTC Elemental Analysis Facility at the University of Rochester, funded by NSF Grant CHE-0650456. We thank K. Cory MacLeod for valuable discussions.

■ REFERENCES

(1) Nielsen, A. *Ammonia: Catalysis and Manufacture*; Springer: Heidelberg, 1995.
(2) Ru catalysts and Co-Mo catalysts also show great promise. See: Schlögl, R. *Angew. Chem., Int. Ed.* **2003**, *42*, 2004.
(3) Schlögl, R. In *Handbook of Heterogeneous Catalysis*, 2nd ed.; Wiley-VCH: Weinheim, 2008; Vol. *5*, p 2501.
(4) (a) Bare, S. R.; Strongin, D. R.; Somorjai, G. A. *J. Phys. Chem.* **1986**, *90*, 4726. (b) Strongin, D. R.; Somorjai, G. A. *Catal. Lett.* **1988**, *1*, 61. (c) Strongin, D. R.; Somorjai, G. A. *J. Catal.* **1988**, *109*, 51. (d) Strongin, D. R.; Somorjai, G. A. *J. Catal.* **1989**, *118*, 99.
(5) (a) Spencer, N. D.; Schoonmaker, R. C.; Somorjai, G. A. *J. Catal.* **1982**, *74*, 129. (b) Strongin, D. R.; Carrazza, J.; Bare, S. R.; Somorjai, G. A. *J. Catal.* **1987**, *103*, 213. (c) Falicov, L. M.; Somorjai, G. A. *Proc. Natl. Acad. Sci. U. S. A.* **1985**, *82*, 2207. (d) Mortensen, J. J.; Hansen, L. B.; Hammer, B.; Nørskov, J. K. *J. Catal.* **1999**, *182*, 479.
(6) (a) Grunze, M.; Golze, M.; Hirschwald, W.; Freund, H. J.; Pulm, H.; Seip, U.; Tsai, M. C.; Ertl, G.; Kueppers, J. *Phys. Rev. Lett.* **1984**, *53*, 850. (b) Freund, H. J.; Bartos, B.; Messmer, R. P.; Grunze, M.; Kuhlenbeck, H.; Neumann, M. *Surf. Sci.* **1987**, *185*, 187.
(7) (a) Mortensen, J. J.; Hansen, L. B.; Hammer, B.; Nørskov, J. K. *J. Catal.* **1999**, *182*, 479. (b) Egeberg, R. C.; Dahl, S.; Logadottir, A.; Larsen, J. H.; Nørskov, J. K.; Chorkendorff, I. *Surf. Sci.* **2001**, *491*, 183. (c) Dahl, S.; Logadottir, A.; Jacobsen, C. J. H.; Nørskov, J. K. *Appl. Catal., A* **2001**, *222*, 19.
(8) (a) Burgess, B. K. *Chem. Rev.* **1990**, *90*, 1377. (b) Burgess, B. K.; Lowe, D. J. *Chem. Rev.* **1996**, *96*, 2983.
(9) (a) Spatzal, T.; Aksoyoglu, M.; Zhang, L.; Andrade, S. L. A.; Schleicher, E.; Weber, S.; Rees, D. C.; Einsle, O. *Science* **2011**, *334*, 940. (b) Lancaster, K. M.; Roemelt, M.; Ettenhuber, P.; Hu, Y.; Ribbe, M. W.; Neese, F.; Bergmann, U.; DeBeer, S. *Science* **2011**, *334*, 974. (c) Wiig, J. A.; Hu, Y.; Lee, C. C.; Ribbe, M. W. *Science* **2012**, *337*, 1672.
(10) (a) Christiansen, J.; Seefeldt, L. C.; Dean, D. R. *J. Biol. Chem.* **2000**, *275*, 36104. (b) Seefeldt, L. C.; Dance, I. G.; Dean, D. R. *Biochemistry* **2004**, *43*, 1401. (c) Dos Santos, P. C.; Igarashi, R. Y.; Lee, H.-I.; Hoffman, B. M.; Seefeldt, L. C.; Dean, D. R. *Acc. Chem. Res.* **2005**, *38*, 208. (d) Hoffman, B. M.; Dean, D. R.; Seefeldt, L. C. *Acc. Chem. Res.* **2009**, *42*, 609. (e) Hoffman, B. M.; Lukoyanov, D.; Yang, Z.-Y.; Dean, D. R.; Seefeldt, L. C. *Chem. Rev.* **2014**, *114*, 4041.
(11) Spatzal, T.; Perez, K. A.; Einsle, O.; Howard, J. B.; Rees, D. C. *Science* **2014**, *345*, 1620.
(12) Krabetz, R.; Peters, C. *Angew. Chem.* **1965**, *77*, 333.
(13) (a) Hidai, M.; Mizobe, Y. *Chem. Rev.* **1995**, *95*, 1115. (b) MacKay, B. A.; Fryzuk, M. D. *Chem. Rev.* **2004**, *104*, 385. (c) Hazari, N. *Chem. Soc. Rev.* **2010**, *39*, 4044. (d) Crossland, J. L.; Tyler, D. R. *Coord. Chem. Rev.* **2010**, *254*, 1883.
(14) For a review on multimetallic activation of N_2, see: Gambarotta, S.; Scott, J. *Angew. Chem., Int. Ed.* **2004**, *43*, 5298.
(15) (a) Scott, J.; Vidyaratne, I.; Korobkov, I.; Gambarotta, S.; Budzelaar, P. H. M. *Inorg. Chem.* **2008**, *47*, 896. (b) Powers, T. M.; Fout, A. R.; Zheng, S.-L.; Betley, T. A. *J. Am. Chem. Soc.* **2011**, *133*, 3336. (c) Powers, T. M.; Betley, T. A. *J. Am. Chem. Soc.* **2013**, *135*, 12289.
(16) Smith, J. M.; Sadique, A. R.; Cundari, T. R.; Rodgers, K. R.; Lukat-Rodgers, G.; Lachicotte, R. J.; Flaschenriem, C. J.; Vela, J.; Holland, P. L. *J. Am. Chem. Soc.* **2006**, *128*, 756.
(17) Chiang, K. P.; Bellows, S. M.; Brennessel, W. W.; Holland, P. L. *Chem. Sci.* **2014**, *5*, 267.
(18) Rodriguez, M. M.; Bill, E.; Brennessel, W. W.; Holland, P. L. *Science* **2011**, *334*, 780.
(19) A new series of Fe compounds can reduce N_2 to ammonia catalytically through simultaneous protonation and reduction. See: (a) Anderson, J. S.; Rittle, J.; Peters, J. C. *Nature* **2013**, *501*, 84. (b) Creutz, S. E.; Peters, J. C. *J. Am. Chem. Soc.* **2014**, *136*, 1105.
(20) (a) Park, J.; Morimoto, Y.; Lee, Y.-M.; Nam, W.; Fukuzumi, S. *J. Am. Chem. Soc.* **2011**, *133*, 5236. (b) Park, Y. J.; Ziller, J. W.; Borovik, A. S. *J. Am. Chem. Soc.* **2011**, *133*, 9258. (c) Kundu, S.; Miceli, E.; Farquhar, E.; Pfaff, F. F.; Kuhlmann, U.; Hildebrandt, P.; Braun, B.; Greco, C.; Ray, K. *J. Am. Chem. Soc.* **2012**, *134*, 14710. (d) Lacy, D. C.; Park, Y. J.; Ziller, J. W.; Yano, J.; Borovik, A. S. *J. Am. Chem. Soc.* **2012**, *134*, 17526. (e) Chen, J.; Lee, Y.-M.; Davis, K. M.; Wu, X.; Seo, M. S.; Cho, K.-B.; Yoon, H.; Park, Y. J.; Fukuzumi, S.; Pushkar, Y. N.; Nam, W. *J. Am. Chem. Soc.* **2013**, *135*, 6388. (f) Herbert, D. E.; Lionetti, D.; Rittle, J.; Agapie, T. *J. Am. Chem. Soc.* **2013**, *135*, 19075.
(21) Ubbelohde, A. R. In *Proceedings of the International Conference on the Physics of Intercalation Compounds*, Pietronero, L. and Tosatti, E., eds., Springer-Verlag, Berlin, 1981.
(22) Ongoing studies are aimed at elucidating the intermediate(s) in these reactions, and the results will be reported in due course.
(23) Ming, L.-J. Nuclear magnetic resonance of paramagnetic metal centers in proteins and synthetic complexes. In *Physical Methods in Bioinorganic Chemistry*; Que, L., Ed.; University Science Books: Sausalito, CA, 2000; p 375.
(24) MacLeod, K. C.; Vinyard, D. J.; Holland, P. L. *J. Am. Chem. Soc.* **2014**, *136*, 10226.
(25) No reaction was observed in benzene, probably because the triflate salts are insoluble.
(26) (a) Huertos, M. A.; Pérez, J.; Riera, L.; Díaz, J.; López, R. *Angew. Chem., Int. Ed.* **2010**, *49*, 6409. (b) Kucheryna, A. *Syntheses and properties of compounds containing the bis(trifluoromethyl)amido group*. Ph.D. Thesis, Universität Wuppertal, Wuppertal, Germany, 2006.
(27) (a) Ebert, L. B. *Annu. Rev. Mater. Sci.* **1976**, *6*, 181. (b) Dresselhaus, M. S.; Dresselhaus, G. *Adv. Phys.* **1981**, *30*, 139. (c) Csuk, R.; Glänzer, B. I.; Fürstner, A. In *Advances in Organometallic Chemistry*; Academic Press: San Diego, 1988; p 85. (d) Yazami, R. *J. Power Sources* **1993**, *43*−*44*, 39. (e) Udod, I. A. *Synth. Met.* **1997**, *88*, 127. (f) Caragiu, M.; Finberg, S. *J. Phys.: Condens. Matter* **2005**, *17*, R995.
(28) We have also performed reactions using K amalgam. No formation of **1-K** was observed, suggesting that amalgams are generally ineffective for these reductions.
(29) Dögens, E. In *Handbook of Preparative Inorganic Chemistry*; Brauer, G., Ed.; Academic Press: London, 1963; Vol. *1*, pp 950−992.
(30) We have also performed a spiking experiment by adding CsCl to test the possibility that this salt gives the observed signal. While the chemical shift of CsCl was similar (0.00 ppm for CsCl vs 0.03 for **4-Cs**), the width (fwhm) was much smaller for CsCl (2.93 Hz vs 226.16 Hz for **4-Cs**).
(31) Stoian, S. A.; Vela, J.; Smith, J. M.; Sadique, A. R.; Holland, P. L.; Münck, E.; Bominaar, E. L. *J. Am. Chem. Soc.* **2006**, *128*, 10181.
(32) Addition of CsOTf to a THF solution of **4-Rb** for 30 min at room temperature did not give any **4-Cs** as judged by ^{1}H NMR spectroscopy, indicating that the alkali metals are not labile in the triangular clusters.
(33) Chaney, A. L.; Marbach, E. P. *Clin. Chem.* **1962**, *8*, 130.
(34) Dougherty, D. A. *Acc. Chem. Res.* **2012**, *46*, 885.
(35) (a) This Re compound has refcode JEHBUU in the CSD. (b) Cambridge Structural Database (CSD): Allen, F. H. *Acta Crystallogr.* **2002**, *B58*, 380. (c) A triangular $FeMo_3(N_2)_3$ compound with three N_2 units radiating from a central three-coordinate Fe is also known: O'Donoghue, M. B.; Davis, W. M.; Schrock, R. R.; Reiff, W. M. *Inorg. Chem.* **1999**, *38*, 243.
(36) Figg, T. M.; Holland, P. L.; Cundari, T. R. *Inorg. Chem.* **2012**, *51*, 7546.
(37) (a) Guillet, G. L.; Sloane, F. T.; Ermert, D. M.; Calkins, M. W.; Peprah, M. K.; Knowles, E. S.; Cizmar, E.; Abboud, K. A.; Meisel, M. W.; Murray, L. J. *Chem. Commun.* **2013**, *49*, 6635. (b) Di Francesco, G. N.; Gaillard, A.; Ghiviriga, I.; Abboud, K. A.; Murray, L. J. *Inorg. Chem.* **2014**, *53*, 4647.

(38) Murray, L. J.; Weare, W. W.; Shearer, J.; Mitchell, A. D.; Abboud, K. A. *J. Am. Chem. Soc.* **2014**, *136*, 13502.
(39) MacLeod, K. C.; Holland, P. L. *Nat. Chem.* **2013**, *5*, 559.
(40) Bailey, P. J.; Coxall, R. A.; Dick, C. M.; Fabre, S.; Henderson, L. C.; Herber, C.; Liddle, S. T.; Loroñzo-González, D.; Parkin, A.; Parsons, S. *Chem.—Eur. J.* **2003**, *9*, 4820.
(41) Kern, R. J. *J. Inorg. Nucl. Chem.* **1962**, *24*, 1105.
(42) Hildebrandt, L.; Dinnebier, R.; Jansen, M. *Inorg. Chem.* **2006**, *45*, 3217.
(43) Dresselhaus, M. S.; Dresselhaus, G. *Adv. Phys.* **1981**, *30*, 139.
(44) *APEX2*, version 2012.4−3; Bruker AXS: Madison, WI, 2012.
(45) Altomare, A.; Burla, M. C.; Camalli, M.; Cascarano, G. L.; Giacovazzo, C.; Guagliardi, A.; Moliterni, A. G. G.; Polidori, G.; Spagna, R. *SIR97: A New Program for Solving and Refining Crystal Structures*; Istituto di Cristallografia, CNR: Bari, Italy, 1999.
(46) Sheldrick, G. M. *SHELXL-2012*; University of Göttingen: Göttingen, Germany, 2012.